Journal of the European Ceramic Society 41 (2021) 6075–6079

Contents lists available at ScienceDirect

Journal of the European Ceramic Society

journal homepage: www.elsevier.com/locate/jeurceramsoc

Short communication

# $Li_7La_3Zr_2O_{12}$ solid electrolyte sintered by the ultrafast high-temperature method

Martin Ihrig [a,b,*], Tarini Prasad Mishra [a], Walter Sebastian Scheld [a], Grit Häuschen [a], Wolfgang Rheinheimer [a], Martin Bram [a], Martin Finsterbusch [a,c,**], Olivier Guillon [a,b,c]

[a] Institute of Energy and Climate Research – Materials Synthesis and Processing, Forschungszentrum Jülich GmbH, 52425, Jülich, Germany
[b] Institute of Mineral Engineering, RWTH Aachen University, Mauerstr. 5, 52064, Aachen, Germany
[c] Helmholtz Institute Münster: Ionics in Energy Storage, Corrensstr. 46, 48149 Münster, Germany

ARTICLE INFO

*Keywords:*
Ultrafast high-temperature sintering
LLZO
Phase analysis
Microstructure
Impedance

ABSTRACT

All-solid-state Li batteries (ASSLBs) are regarded as the systems of choice for future electrochemical energy storage. Particularly, the garnet $Li_7La_3Zr_2O_{12}$ (LLZO) is one of the most promising solid electrolytes due to its stability against Li metal. However, its integration into ASSLBs is challenging due to high temperature and long dwell time required for sintering. Advanced sintering techniques, such as Ultrafast High-temperature Sintering, have shown to significantly increase the sintering rate. Direct contact to graphite heaters allows sintering of LLZO within 10 s due to extremely high heating rates (up to $10^4$ K $min^{-1}$) and temperatures up to 1500 °C to a density around 80 %. The LLZO sintered in vacuum and Ar atmosphere has good mechanical stability and high phase purity, but kinetic de-mixing at the grain boundaries was observed. Nevertheless, the Li-ion conductivity of 1 mS $cm^{-1}$ at 80 °C was comparable to conventional sintering, but lower than for Field-Assisted Sintering Technique/ Spark Plasma Sintering.

## 1. Introduction

Li-ion batteries are the most important electrochemical energy storage system powering our portable electronic devices. They also become the system of choice for smaller stationary storage devices and electric vehicles, as they offer high energy density, lightweight design, and longer lifetime than other battery types [1–3]. However, with the increasing energy density and capacity of Li-ion batteries, safety concerns arise due to flammable liquid electrolytes. To circumvent this issue, solid oxide Li-ion conductors can be used to develop All-Solid-State Lithium Batteries (ASSLBs). The lack of liquid electrolytes results in intrinsic safety, extended operational temperature and potentially higher energy densities [1,2]. One of the most promising solid electrolytes is the garnet-type $Li_7La_3Zr_2O_{12}$ (LLZO) [2,4]. While the high Li-ion conductivity of LLZO and its stability against Li metal make are attractive properties, the processing of LLZO is challenging and its integration in battery cells hampers the development of LLZO-based ASSLBs.

In order to obtain a good contact between individual LLZO grains and high Li-ion conductivity, conventional sintering at temperature above 1050 °C and dwell time of many hours are required [1,2]. Such extended heat treatment causes chemical instability LLZO e.g. by Li loss or chemical reactions particularly in contact with the Cathode Active Material (CAM). Promising CAMs such as $Li[Ni_{1-x-y}Mn_xCo_y]O_2$ (NMC) or $Li_2NiMn_3O_8$ (NMO) are thermodynamic not stable when processed in contact with LLZO [5]. The oxidizing nature of CAMs prompts the reaction with LLZO already at about 700 °C for NMC and at 500 °C for NMO, which is far below the sintering temperature of LLZO [6].

It was shown that an optimized sintering process with shorter heating times can help overcome or significantly reduce chemical reactions [7–10]. Recently, a new sintering technology called Ultrafast High-temperature Sintering (UHS) was reported by Wang et al. to sinter LLZO [11]. UHS uses an electric current to heat a carbon felt by Joule heating within seconds to temperatures up to 3000 °C [11]. As the specimen is in direct contact to the carbon felt, the heat is rapidly transferred, resulting in a heating rate of $10^3$ to $10^4$ K$min^{-1}$ and to reach

* Corresponding author at: Institute of Energy and Climate Research – Materials Synthesis and Processing, Forschungszentrum Jülich GmbH, 52425, Jülich, Germany.
** Corresponding author.
*E-mail addresses:* m.ihrig@fz-juelich.de (M. Ihrig), m.finsterbusch@fz-juelich.de (M. Finsterbusch).

https://doi.org/10.1016/j.jeurceramsoc.2021.05.041
Received 16 April 2021; Received in revised form 13 May 2021; Accepted 20 May 2021
Available online 24 May 2021

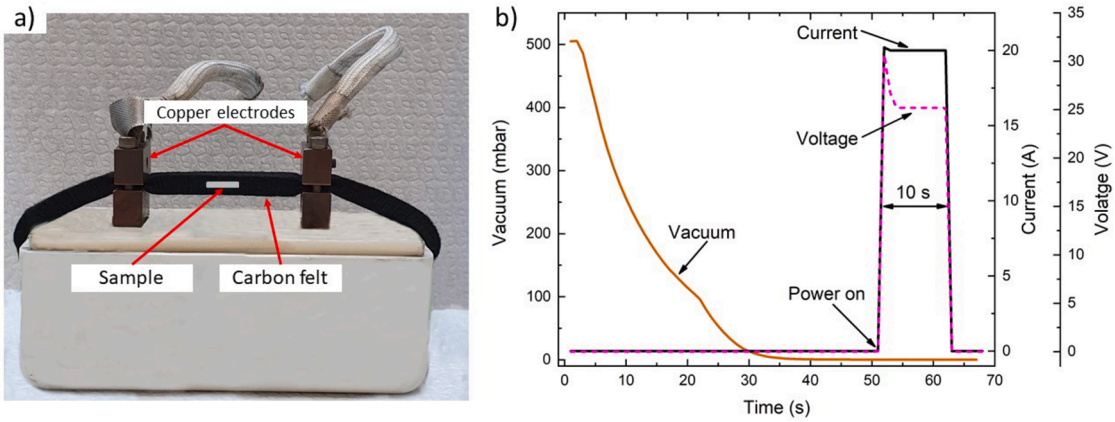


**Fig. 1.** a) UHS experimental setup showing the position of the LLZO:Ta pellet shaped sample in the cut of the carbon felt. The setup was operated under vacuum or Ar and an electric current was applied through the copper electrodes. The UHS process parameters for the maximum current of 20 A are shown in b). The power supply was switched on only for 10 s, therefore, the UHS-sintering cycle was completed in 10 s.

very high temperatures within few seconds [11]. The high heating rate and short processing time help avoiding the formation of volatile phases such as Li [12].

In this work, we demonstrate that UHS can be used to sinter bulk LLZO pellets without the need of sintering additives. It is shown that the atmosphere chosen for UHS (here Ar and vacuum) can influence the phase purity of LLZO. Analysis of the microstructure and the Li-ion conductivity of the UHS-sintered LLZO was used for characterization of the resulting grain structure. The Li-ion conductivity is comparable to conventional sintering processes but lower than for Field-Assisted Sintering Technique/Spark Plasma Sintering (FAST/SPS). This is possibly caused by kinetic de-mixing at the grain boundaries. A detailed impedance analysis indicates potential to further improve the conductivity by optimizing the microstructure.

## 2. Experimental procedures

A custom made Ultrafast High-temperature Sintering (UHS) setup was used, containing two copper electrodes and a carbon felt (SGL CARBON GmbH, 10 mm wide and 4 mm thick) clamped between the electrodes. The distance between the electrodes was approximately 45 mm. A very fine cut was made at the center of the carbon felt with a scalpel, and the pellet-shaped samples were placed in the cut (Fig. 1a). The samples were prepared from LLZO:Ta powder ($Li_{6.45}Al_{0.05}La_3Zr_{1.6}Ta_{0.4}O_{12}$ [13]). The powder was uniaxially pressed (height: 1 mm, diameter: 8 mm) to a green density of 68 %. The UHS setup was operated with an AC/DC power source (TruPlasma Bipolar Series 4000, Trumpf Hüttinger) and was placed in a vacuum chamber allowing to control of the atmosphere (vacuum or Ar). The electric current was applied to the carbon felt via the electrodes, resulting in a very fast heating of the carbon felt within a second. The maximum current was held for 10 s. As an example, Fig. 1b shows the UHS processing parameters for a current of 20 A in vacuum. Due to the very high heating rates, the sample temperature cannot be measured adequately and remains inaccessible as in other high high heating rate processes [14,15].

The sintered LLZO:Ta pellets were characterized regarding their density, microstructure, phase purity, and Li-ion conductivity. The density of the pellets was determined by the Archimedes method using a theoretical density of 5.3 g $cm^{-3}$ for LLZO:Ta [16]. After polishing of the surface with water-free diamond suspension (1 µm, Buehler), the microstructure was investigated by Scanning Electron Microscopy (SEM) in backscattering mode and Energy Dispersive X-ray spectroscopy (EDX, TM3000, Hitachi). The mean grain size was quantified by the linear intercept method considering around 20 grains for each value. Raman spectroscopy (inVia Qontor, Renishaw) was performed using a solid-state 532 nm excitation laser with 60 mW, 2400 L $mm^{-1}$ grating and a 100x objective on polished surfaces (as prepared for SEM). The Li-ion conductivity was measured between -60 °C and 80 °C by Electrochemical Impedance Spectroscopy (EIS, Alpha-a, Novocontrol) and fitted with the software "ZView" (Scribner Associates Inc.). For the EIS measurements, the LLZO:Ta pellets were ground with SiC paper (grade #4000) and sputter-coated with Au for 150 s (Cressington 108 sputter coater). The sample thickness was 1.09 mm (vacuum) and 1.1 mm (Ar).

**Table 1**
Densities of the UHS-sintered LLZO:Ta pellets.

| Sintering conditions | Absolute density (g $cm^{-3}$) | Relative density (%) |
|---|---|---|
| vacuum, 16 A | 4.19 | 79 |
| vacuum, 18 A | 4.20 | 79 |
| vacuum, 20 A | 4.37 | 82 |
| vacuum, 22 A | 4.95 | 93 |
| Ar, 20 A | 4.29 | 81 |

## 3. Results

The LLZO:Ta ($Li_{6.45}Al_{0.05}La_3Zr_{1.6}Ta_{0.4}O_{12}$) pellets maintained their shape during UHS and the linear shrinkage was around 7 % for 20 A in vacuum and Ar (further denoted as UHS-vac and UHS-Ar). A density of 80 ± 2 % was obtained in the case of UHS-vac pellets sintered at currents between 16 A and 20 A, In the case of UHS-Ar pellets, same density was achieved at 20 A (Table 1). A higher density of 93 % was obtained when increasing the current to 22A, likely due to a partial melting. The melting temperature of LLZO is between 1500 °C and 1700 °C [12]. Decreasing the current below 16 A led to poor sintering and mechanical stability.

Microstructural analysis was performed for the UHS-vac and UHS-Ar pellets sintered at 20 A (Fig. 2a and b). All grains appear isometric and almost spherical, although the pristine powder is more irregularly shaped (Supporting Information Fig. S1). FAST/SPS sintered pellets with similar density of 81 % have a more irregular grain morphology as well (Supporting Information Fig. S2). The change in grain morphology hints on a change in the sintering mechanism when directly comparing UHS and FAST/SPS. As high temperatures generally result in more isotropic grain shapes [17], the more isotropic microstructure after UHS could be due to higher sintering temperature than in FAST/SPS.

The mean grain size is about 12 µm and appears to be slightly larger than for the pristine powder ($D_{50}$ of about 10 µm, and Supporting Information Fig. S1) [10]. In contrast, FAST/SPS sintering of LLZO:Ta mostly maintains the grain size distribution and morphology of the starting powder. The increase of the mean grain size after UHS indicates a coarsening of the smallest powder particles. As the density of around

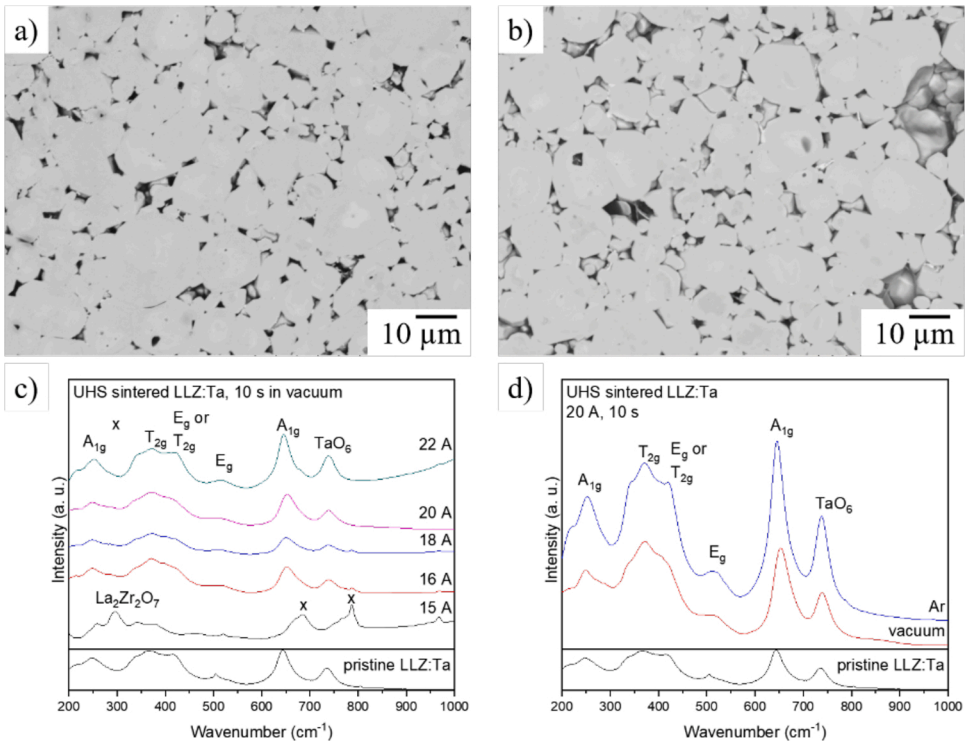


**Fig. 2.** SEM images in backscattering mode of the polished LLZO:Ta pellets sintered in vacuum (a) and Ar atmosphere (b) with a current of 20 A for 10 s. The darker areas are pores. c) The Raman spectra of LLZO:Ta pellets sintered by UHS for 10 s at various currents in vacuum. The two peaks in the spectrum of the sample sintered at 15 A are attributed to the formation of $La_2Zr_2O_7$ as secondary phase (X). d) Application of Ar atmosphere tend to result in a more defined crystal structure of LLZO. The Raman modes are labeled according to [8,22].

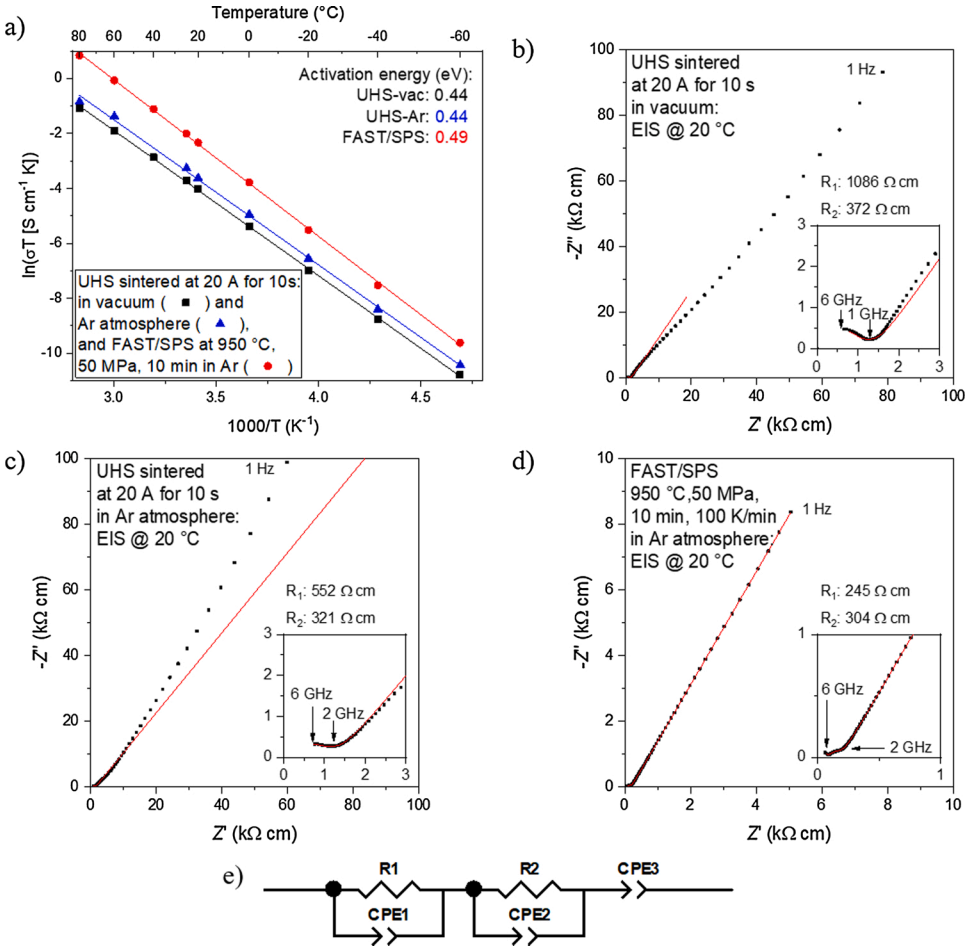


**Fig. 3.** a) Arrhenius plots of the conductivity of LLZO:Ta pellets sintered by UHS (10 s at 20 A) in vacuum and Ar atmosphere. The EIS spectra (dots) at 20 °C of samples sintered in vacuum and Ar atmosphere are shown in (b) and)c). In comparison, the EIS spectra of LLZO:Ta sintered by FAST/SPS is displayed in d). The equivalent circuit for the fits (lines) is shown in e). R denotes an ohmic resistor and CPE a constant phase element.

81 % is unlikely to allow grain growth by grain boundary migration due to pore drag [18], coarsening of the smallest particles likely occurred either due to surface diffusion or evaporation and condensation as in other ceramic materials like SiC [18] or KNN [19].

For UHS-vac and UHS-Ar (both sintered at 20 A), residual porosity is evident considering the relative density of 81 % (Fig. 2). For further optimization of microstructure and density, the heating rate and electric current need to be optimized further and the LLZO:Ta powder needs to be tailored for the process. Beyond this, the sintering temperature of LLZO:Ta, can be lowered either by substitution with Ga instead of Ta [9] or by using fine-grained powder [9,20].

Raman spectroscopy is a fingerprint method to analyze the phase composition and structure of LLZO:Ta. The Raman spectra of the LLZO:Ta powder and sintered UHS-vac and UHS-Ar pellets are shown in Fig. 2c and d. The cubic structure of the LLZO:Ta was found for all UHS pellets sintered above 15 A (Fig. 2c). For UHS-vac sintered at 15 A, the $La_2Zr_2O_7$ signal dominates the spectrum. Hence, it can be assumed that the applied current of 15 A heats LLZO:Ta to a temperature between 450 °C and 750 °C, in which the formation of the pyrochlore $La_2Zr_2O_7$ phase is observed in the case of conventional sintering [21]. Currents above 15 A lead to higher processing temperatures and therefore prevent the formation of pyrochlore $La_2Zr_2O_7$ phase. Instead, the desired cubic LLZO:Ta structure is obtained. However, if the current is too high, LLZO:Ta likely starts to melt as observed for a current of 22 A. The melting and subsequent rapid solidification also impacts the crystal structure as indicated by a slight distortion of the Raman spectra of the 22 A sample, particularly between 300 $cm^{-1}$ and 500 $cm^{-1}$. This distortion could indicate by a change in chemical composition during solidification or the occurrence of residual thermal stress due to rapid cooling.

Sintering in vacuum, however, might not be the optimum atmosphere when aiming on co-sintering of LLZO:Ta with CAMs, e.g. $LiCoO_2$. Laptev et al. reported a higher thermal stability when sintering a LLZO:Ta and $LiCoO_2$ mixture in Ar atmosphere [7]. In addition, Ping et al. argued that evaporation of volatile elements like Li is expected to decrease in Ar atmosphere due to a higher atmospheric pressure [12]. In the present study, UHS-sintering of LLZO:Ta in Ar atmosphere maintained the cubic crystal structure slightly better than in vacuum (as indicated by the Raman spectra in Fig. 2d). This suggests that the structure and phase purity of LLZO:Ta sintered by UHS is also affected by the atmosphere, and Ar is beneficial for the phase purity, likely by decreasing the evaporation of Li.

The Li-ion conductivity of the UHS-vac and UHS-Ar pellets sintered at 20 A, and – as reference – of a pellet sintered by FAST/SPS (950 °C, 50 MPa, 10 min in Ar) was measured by EIS between -60 °C and 80 °C (Fig. 3a). For UHS-vac, a total Li-ion conductivity of only 0.08 mS $cm^{-1}$ was measured at room temperature (RT), while for UHS-Ar, a total Li-ion conductivity of 0.12 mS $cm^{-1}$ was obtained. Even if the density was similar (81 %), the LLZO:Ta sintered by FAST/SPS achieved a total Li-ion conductivity of 0.45 mS $cm^{-1}$. The lower total Li-ion conductivity for the same chemical composition, a similar relative density and only slightly larger grain sizes likely indicates a change in the grain boundary properties by UHS compared to FAST/SPS. At elevated temperatures (80 °C), the total Li-ion conductivity of UHS-sintered LLZO:Ta is 1 mS $cm^{-1}$ similar to conventionally sintered LLZO [23]. A value of 1 mS $cm^{-1}$ is considered as the minimum total Li-ion conduction required for an application in ASSLB [4]. The activation energy of Li ion conduction is 0.44 eV for UHS-vac and UHS-Ar, which is similar to conventionally sintered LLZO:Ta with cubic structure [16].

EIS measurements at 20 °C were fitted to separate the grain and grain boundary contributions to the impedance (Fig. 3b to d). The semicircle at high (low) frequencies involves a capacity in the range $10^{-12}$ F ($10^{-10}$ F) and are assumed as grain (grain boundary) contribution [24]. The diffusion tail in the low frequency range is a result of Li-ion diffusion into the Au electrodes of the impedance setup [25]. At 20 °C, the Li-ion conductivity of the grains is one order of magnitude higher than the grain boundary conductivity (Supporting Information Tab. S1 and S2). However, the grain boundary conductivity of LLZO at 20 °C should be similar or even higher than the bulk conductivity [26]. This indicates that in the present study the Li-ion conductivity is limited by the grain boundary conductivity.

As detailed in the supporting information, the impedance analysis allows approximating the average capacity, resistance and thickness of the low conducting layers of an individual grain boundary (Supporting

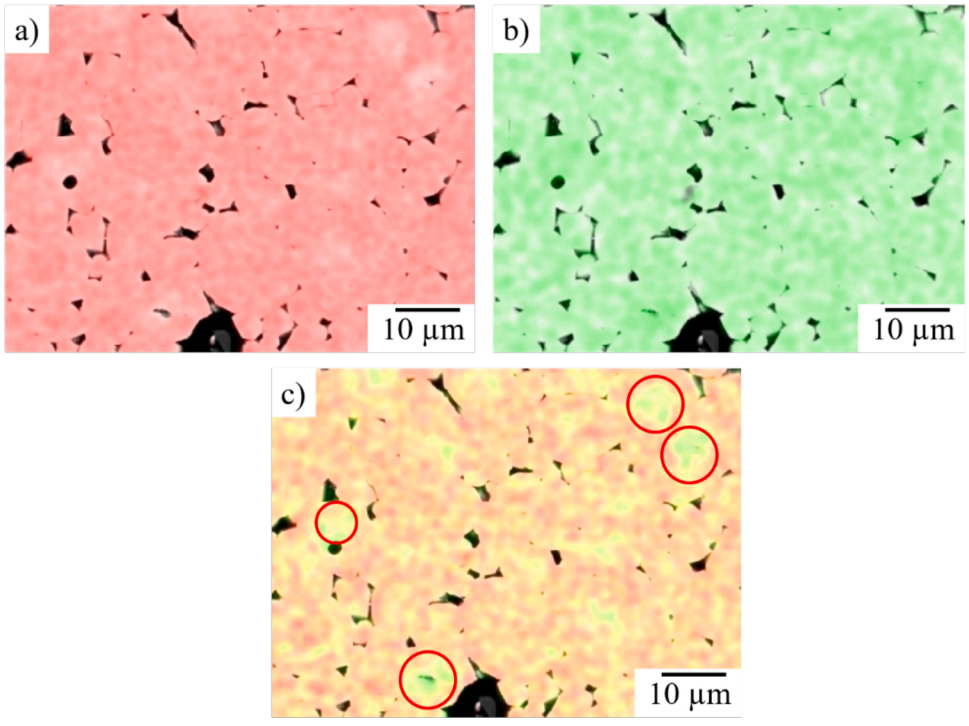


**Fig. 4.** EDX mapping of (a) Zr, (b) Ta, and as overlap in c) for the UHS-vac at 20 A. Kinetic de-mixing can be observed in some highlighted areas by (circles) in (c).

Information Tab. S3). At 20 °C, the obtained grain boundary layer thickness ranges from 13 nm (FAST/SPS) up to 67 nm (UHS). The low grain boundary thickness of a few tenth nm agrees well with typical thickness of space charge layers [27–29]. Compared to FAST/SPS, the grain boundary thickness and resistance are higher for UHS-vac and UHS-Ar. Likely, the high grain boundary thickness and low grain boundary conductivity of the UHS sintered LLZO:Ta is caused by a chemical inhomogeneity as indicated by EDX (Fig. 4). The particles show a core-shell structure of the chemical composition. Some inhomogeneity in the distribution of Zr and Ta was observed and might be due to kinetic de-mixing during the rapid heating and cooling even if only a single phase was determined by Raman spectroscopy (Fig. 2). Inada et al. reported an increasing total Li-ion conductivity with Ta substitution of Zr in LLZO [16]. Therefore, loss of Ta close to the grain boundary might explain the low grain boundary conductivity.

## 4. Conclusion

UHS allows the sintering of LLZO:Ta within a few seconds offering new pathways for the processing and sintering of electrolytes for ASSLBs. The short exposure time to high temperature reduces the loss of Li by evaporation, and therefore offering the possibility to lower the need of Li excess during synthesis and of a co-firing with CAMs. Potentially, this new kind of sintering enables a more competitive and environmentally friendly processing of LLZO:Ta electrolytes for ASSLBs, particularly due to significant energy saving during the sintering.

The sintering atmosphere was found to significantly influence the microstructure evolution, and a lot of potential for further optimization still exists. A dense and highly conductive polycrystalline crystal structure of LLZO:Ta was obtained by UHS in only 10 s. At elevated temperature of 80 °C a total Li-ion conductivity of 1 mS $cm^{-1}$ is achieved, which is comparable to the conductivity of conventionally sintered LLZO, but lower than the conductivity of FAST/SPS samples [2]. After consolidation by UHS, slight grain coarsening and indication of kinetic de-mixing at grain boundaries were observed. A careful impedance analysis has proven a lower grain boundary conductivity, which is likely caused by the chemical inhomogeneity coupled with the kinetic de-mixing. This finding points towards pathways of further process and microstructure optimization to gain higher conductivities by UHS.

The short processing time of only 10 s of UHS offers immense potential for co-sintering of LLZO:Ta and CAMs. In conventional sintering, long dwell time at high temperature often leads to the decomposition of the CAM in contact with LLZO:Ta, which might be avoided by UHS processing [5]. However, the effect of the kinetic de-mixing observed for LLZO:Ta could vice versa negatively impact the LLZO:Ta/CAM interface properties. Beyond ASSLBs, UHS offers new pathways for the densification of multiphase materials and systems where chemical reactions and inter-diffusion limit conventional sintering processes.

## Declaration of Competing Interest

The authors declare no competing financial interest.

## Acknowledgements

Financial support by the German Federal Ministry of Education and Research under project No. 13XP0134A (EvaBatt), 13XP0305A (AdamBatt) and 13XP0173A (FestBatt-Oxide) is gratefully acknowledged. Financial support from the German Research Foundation (DFG) within the Priority Program on “Manipulation of matter controlled by an electric and magnetic field, SPP 1959 under the Grant No. BR 3418/1-2, and within the Emmy Noether Program under Grant No. Rh 146/1-1.

## Appendix A. Supplementary data

Supplementary material related to this article can be found, in the online version, at doi:https://doi.org/10.1016/j.jeurceramsoc.2021.05.041.

## References

[1] N. Zhao, W. Khokhar, Z. Bi, C. Shi, X. Guo, L.-Z. Fan, C.-W. Nan, Joule 3 (2019) 1190–1199.
[2] C. Wang, K. Fu, S.P. Kammampata, D.W. McOwen, A.J. Samson, L. Zhang, G. T. Hitz, A.M. Nolan, E.D. Wachsman, Y. Mo, V. Thangadurai, L. Hu, Chem. Rev. 120 (2020) 4257–4300.
[3] C. Wang, K. Fu, S.P. Kammampata, D.W. McOwen, A.J. Samson, L. Zhang, G. T. Hitz, A.M. Nolan, E.D. Wachsman, Y. Mo, V. Thangadurai, L. Hu, Chem. Rev. (2020).
[4] V. Thangadurai, S. Narayanan, D. Pinzaru, Chem. Soc. Rev. 43 (2014) 4714–4727.
[5] L. Miara, A. Windmuller, C.L. Tsai, W.D. Richards, Q.L. Ma, S. Uhlenbruck, O. Guillon, G. Ceder, ACS Appl. Mater. Interfaces 8 (2016) 26842–26850.
[6] Y. Ren, T. Liu, Y. Shen, Y. Lin, C.-W. Nan, J. Mater. 2 (2016) 256–264.
[7] A.M. Laptev, H. Zheng, M. Bram, M. Finsterbusch, O. Guillon, Mater. Lett. 247 (2019) 155–158.
[8] C.-L. Tsai, Q. Ma, C. Dellen, S. Lobe, F. Vondahlen, A. Windmüller, D. Grüner, H. Zheng, S. Uhlenbruck, M. Finsterbusch, F. Tietz, D. Fattakhova-Rohlfing, H. P. Buchkremer, O. Guillon, Sustain. Energy Fuels (2019) 280–291.
[9] R. Pfenninger, M. Struzik, I. Garbayo, E. Stilp, J.L.M. Rupp, Nat. Energy 4 (2019) 475–483.
[10] M. Ihrig, M. Finsterbusch, C.-L. Tsai, A.M. Laptev, C.-h. Tu, M. Bram, Y.J. Sohn, R. Ye, S. Sevinc, S.-k. Lin, D. Fattakhova-Rohlfing, O. Guillon, J. Power Sources 482 (2021), 228905.
[11] C. Wang, W. Ping, Q. Bai, H. Cui, R. Hensleigh, R. Wang, A.H. Brozena, Z. Xu, J. Dai, Y. Pei, C. Zheng, G. Pastel, J. Gao, X. Wang, H. Wang, J.-C. Zhao, B. Yang, X. Zheng, J. Luo, Y. Mo, B. Dunn, L. Hu, Science 368 (2020) 521–526.
[12] W. Ping, C. Wang, R. Wang, Q. Dong, Z. Lin, A.H. Brozena, J. Dai, J. Luo, L. Hu, Sci. Adv. 6 (2020), eabc8641.
[13] C.L. Tsai, V. Roddatis, C.V. Chandran, Q. Ma, S. Uhlenbruck, M. Bram, P. Heitjans, O. Guillon, ACS Appl. Mater. Interfaces 8 (2016) 10617–10626.
[14] W. Ji, B. Parker, S. Falco, J.Y. Zhang, Z.Y. Fu, R.I. Todd, J. Eur. Ceram. Soc. 37 (2017) 2547–2551.
[15] F. Lemke, W. Rheinheimer, M.J. Hoffmann, Scr. Mater. 130 (2017) 187–190.
[16] R. Inada, K. Kusakabe, T. Tanaka, S. Kudo, Y. Sakurai, Solid State Ion. 262 (2014) 568–572.
[17] W. Rheinheimer, M. Bäurer, H. Chien, G.S. Rohrer, C.A. Handwerker, J.E. Blendell, M.J. Hoffmann, Acta Mater. 82 (2015) 32–40.
[18] M.N. Rahaman, Ceramic Processing and Sintering, 2nd ed., Dekker, 2003.
[19] J. Acker, H. Kungl, R. Schierholz, S. Wagner, R.-A. Eichel, M.J. Hoffmann, J. Eur. Ceram. Soc. 34 (2014) 4213–4221.
[20] J.S. Park, L. Cheng, V. Zorba, A. Mehta, J. Cabana, G. Chen, M.M. Doeff, T. J. Richardson, J.H. Park, J.-W. Son, W.-S. Hong, Thin Solid Films 576 (2015) 55–60.
[21] G. Larraz, A. Orera, M.L. Sanjuán, J. Mater. Chem. A 1 (2013) 11419–11428.
[22] F. Tietz, T. Wegener, M.T. Gerhards, M. Giarola, G. Mariotto, Solid State Ion. 230 (2013) 77–82.
[23] N. Janani, C. Deviannapoorani, L. Dhivya, R. Murugan, RSC Adv. 4 (2014) 51228–51238.
[24] J.T.S. Irvine, D.C. Sinclair, A.R. West, Adv. Mater. 2 (1990) 132–138.
[25] M. Amores, H. El-Shinawi, I. McClelland, S.R. Yeandel, P.J. Baker, R.I. Smith, H. Y. Playford, P. Goddard, S.A. Corr, E.J. Cussen, Nat. Commun. 11 (2020) 6392.
[26] W.E. Tenhaeff, E. Rangasamy, Y. Wang, A.P. Sokolov, J. Wolfenstine, J. Sakamoto, N.J. Dudney, ChemElectroChem 1 (2014) 375–378.
[27] G. Gregori, R. Merkle, J. Maier, Prog. Mater. Sci. 89 (2017) 252–305.
[28] R. Waser, R. Hagenbeck, Acta Mater. 48 (2000) 797–825.
[29] P.C. McIntyre, J. Am. Ceram. Soc. 83 (2000) 1129–1136.